Cold collisions of N (^4S) atoms and NH ($^3\Sigma$) molecules in magnetic fields

Piotr S. Żuchowski and Jeremy M. Hutson
(Dated: August 8, 2010)

We calculate the interaction potential between N atoms and NH molecules and use it to investigate cold and ultracold collisions important for sympathetic cooling. The ratio of elastic to inelastic cross sections is large over a wide range of collision energy and magnetic field for most isotopic combinations, so that sympathetic cooling of NH molecules by N atoms is a good prospect. However, there are important effects due to a p-wave shape resonance that may inhibit cooling in some cases. We show that scaling the reduced mass used in the collision is approximately equivalent to scaling the interaction potential. We then explore the dependence of the scattering properties on the reduced mass and explain the resonant effects observed using angular-momentum-insensitive quantum defect theory.

I. INTRODUCTION

At temperatures below about 1 mK, atoms and molecules enter a fully quantal regime where their de Broglie wavelength is large compared to molecular dimensions. In this regime, collision cross sections and reaction rates are dominated by long-range forces [1, 2] and resonance phenomena [3]. It is likely to be possible to *control* reaction rates by tuning scattering resonances with applied electric and magnetic fields [4–6]. At even lower temperatures, below about 1 μK, trapped atoms and molecules form *quantum gases* such as Bose-Einstein condensates and Fermi-degenerate gases, in which every molecule occupies the lowest allowed translational state in the trap. The quantum gas regime offers additional possibilities for a new form of quantum control, in which chemical transformations are carried out coherently on entire samples of ultracold atoms and molecules.

There have been enormous advances towards these goals in the last few years. In particular, it is now possible to produce ultracold alkali metal dimers in their rovibronic ground states from ultracold atoms both by photoassociation [7–9] and by magnetoassociation followed by stimulated Raman adiabatic passage (STIRAP) [10, 11]. However, for an alkali metal dimer even the ground rovibronic state has nuclear spin hyperfine structure [12, 13], and the resulting splittings are comparable to the kinetic energies involved in ultracold collisions. For the case of ^{40}K^{87}Rb, microwave transitions have been used to transfer the ground-state molecules selectively between different hyperfine and Zeeman levels [10, 14]. In a very recent development, Ospelkaus *et al.* [15] have studied reactive collisions of such state-selected molecules, both with one another and with ultracold K and Rb atoms. They observed remarkable selectivity of the resulting reactions, in which flipping the spin of a single nucleus could cause dramatic changes in the outcome of a collision [16].

Methods that form molecules from ultracold atoms can be applied only in cases where the atoms themselves can be cooled. In practice this restricts them to the alkali metals, the alkaline earths, and a few other elements. These species have a fairly limited chemistry. In order to cool a wider class of molecules, including polyatomic ones, a number of *direct* cooling methods [17–21] have been established over the last decade. Among these methods, *buffer-gas cooling* is based on the particularly simple idea of cooling molecules by elastic collisions with cold He gas. If the molecules are paramagnetic and in low-field-seeking states, they can be confined in a magnetic trap. The temperatures which can be achieved in buffer gas cooling method are limited by the vapour pressure of the buffer gas (ca. 400 mK for ^{3}He), but the method is particularly valuable for two reasons: (i) it is very general and can in principle be applied to any paramagnetic species, provided that a detection scheme is available; (ii) it can produce large numbers and high densities of cold molecules. Buffer-gas cooling has been reported for a variety of molecules including CaH [18], CaF [22], NH [23, 24] , CrH and MnH [25] and also for a number of paramagnetic atoms [26–28]. Buffer-gas cooling followed by evaporative cooling has recently been used to achieve Bose-Einstein condensation with no laser cooling for metastable helium [29].

The direct methods established so far are limited to temperatures of 10 to 100 mK and above. To cool the molecules further, to the μK regime, second-stage cooling methods must be developed. The most promising and conceptually the simplest method is *sympathetic cooling*, in which the molecules are cooled by collisions with an atomic gas that can itself be cooled to the ultracold regime, such as an alkali metal. The most robust trapping methods for molecules work for low-field-seeking states, which are never the lowest possible state in an applied field. Inelastic collisions can therefore occur, and either heat the trapped system or eject the molecules from the trap. Sympathetic cooling can thus be successful only if elastic collisions dominate inelastic ones, and it is usually stated that the ratio of elastic to inelastic cross sections must be 100 or more. Sympathetic cooling was initially developed as a cooling method for trapped ions [30]. More recently it has been used to achieve sub-Kelvin temperatures for polyatomic ions [31] and has also been used to produce ultracold neutral atoms with scattering properties that are not suitable for evaporative cooling, such as ^{41}K [32].

Sympathetic cooling for molecules has not yet been achieved, but several proposals have been explored. It was initially proposed for NH molecules colliding with Rb atoms [33] and studied in more details by Lara *et al.* [34, 35] for OH colliding with Rb. Both OH and NH molecules interact very strongly with Rb and the anisotropy of the interaction potential is large compared to the molecular rotational constant. The large anisotropy implies large couplings between channels with different n (monomer rotation angular momentum) and L (end-over-end angular momentum) quantum num-

bers, and Lara *et al.* showed that this resulted in large inelastic cross-sections in the ultracold regime. The remedies they suggested to improve sympathetic cooling and decrease inelastic cross sections were: (i) to use light atoms as coolants, in order to increase the heights of centrifugal barriers and suppress inelastic channels; (ii) to find atom-molecule system with much smaller anisotropy in the interaction potential.

Soldán *et al.* [36] considered the possibility of reducing the anisotropy by using alkaline-earth atoms (Ae) as collision partners for NH molecules. They showed that the neutral states of Ae–NH systems are coupled to ion-pair states Ae^+NH^-, with crossings between the neutral and ion-pair surfaces at linear geometries. For Sr and Ca atoms the crossings occurs at energies below the atom-molecule threshold, so will be accessible in low-energy collisions. However, for Be-NH and Mg-NH the crossings occurs at energies more than 1000 cm^{-1} above the atom-molecule threshold. In these systems, the ion-pair state is likely to be inaccessible, so it is reasonable to carry out collision calculations on a single covalent surface. In addition, the potential energy surface for Mg–NH turned out to be only weakly anisotropic. Wallis and Hutson [37] carried out quantum scattering calculations of spin relaxation collisions (in magnetic fields) and showed that sympathetic cooling of NH by collisions with Mg atoms should be achievable if the molecules can be precooled to about 10 mK.

Sympathetic cooling has also been considered for NH_3 and ND_3. In this case the molecules are initially slowed in a Stark decelerator [38]. Żuchowski *et al.* [39] surveyed the interaction potentials for NH_3 interacting with alkali-metal and alkaline-earth atoms. Żuchowski and Hutson [40] then carried out quantum scattering calculations on collisions of ND_3 with Rb atoms and showed that molecules that are initially in the upper component of the ammonia inversion doublet are likely to undergo fast collisional relaxation to the ground state, and that this is likely to prevent sympathetic cooling of molecules trapped in low-field-seeking states in an electrostatic trap [41]. However, there is a good prospect for sympathetic cooling of ammonia molecules in high-field-seeking states, even with magnetically trapped atoms, because the terms in the hamiltonian that might cause spin-changing collisions of the Rb atoms are very small. High-field-seeking states of ND_3 can be confined in an alternating current trap [42].

Recently, Hummon *et al.* [43] demonstrated buffer-gas cooling and trapping of N (^{4}S) atoms and simultaneous cotrapping of NH molecules. Subsequent work [44] has demonstrated N atom densities around 5×10^{12} cm^{-3} and lifetimes around 10 s. This offers the possibility of cooling the atoms further with atomic evaporative cooling, which has already been achieved for metastable helium and Cr atoms [45, 46].

A gas of N atoms is potentially an excellent coolant for a sympathetic cooling experiment. The N atom has a very small polarizability compared to Group I and Group II elements and this results in low C_6 coefficients and small anisotropies of the interaction potentials with molecules. The N atom also has a relatively low mass, which results in higher centrifugal barriers and stronger suppression of inelasticity for particles scattered with $L > 0$.

This paper presents theoretical studies of cold and ultracold collisions of N atoms with NH molecules, in order to investigate the possibility of sympathetic cooling of NH by atomic nitrogen. Since the cross sections depend strongly on the reduced mass of the collision system, we consider four isotopic combinations of N–NH systems, with each of the two N atoms being either ^{14}N or ^{15}N. We assume that both N and NH are initially in their magnetically trappable spin-stretched states, with the maximum possible values of the electron spin projection numbers. For such states only spin relaxation (and not spin exchange) can occur and only the sextet interaction potential contributes. We report calculations of the sextet potential for N–NH and explore the behaviour of cross sections as a function of collision energy and magnetic field. We discuss the sensitivity of the scattering results with respect to uncertainties in the interaction potential. Finally, we analyze the behaviour of the shape resonances in terms of angular-momentum-insensitive quantum-defect theory (AQDT) [47].

II. N–NH POTENTIAL

The total spin of the N(^{4}S) + NH($^3\Sigma^-$) system can be $\frac{5}{2}$, $\frac{3}{2}$ or $\frac{1}{2}$. The chemical reaction N + NH $\rightarrow$ N_2 + H, which occurs principally on the doublet surface, has been studied in detail by Varandas and coworkers [48–50] and by Francombe and Nyman [51]. It was shown that the doublet N–NH system forms an N_2H complex without a potential barrier along the minimum energy path. A very small barrier exists between the N_2H complex and N_2 + H products and overall the reaction of forming N_2+H yields 6.33 eV of energy. To our knowledge, no studies of quartet or sextet states of N–NH have been published, though we are aware of work in progress by Tscherbul and coworkers [52].

To obtain the sextet interaction potential we applied the recently developed explicitly correlated, unrestricted coupled-cluster method with single, double and noniterative triple excitations [UCCSD(T)] [53–55]. We used the aug-cc-pVTZ basis set of Peterson *et al.* [56], which is designed specifically for use with explicitly correlated calculations. The results from the explicitly correlated (F12) calculation are compared with those from UCCSD(T) calculations with uncorrelated basis sets in Table I: it may be seen that the explicitly correlated approach dramatically reduces the error caused by using unsaturated basis sets. A fixed NH bond length of 1.0367 Å was used in all the calculations.

The potential energy surface was obtained by carrying out explicitly correlated UCCSD(T) calculations on a grid in Jacobi coordinates (R_i, θ_j), where R is the intermolecular distance measured to the NH center of mass and θ is the angle between the NH bond vector and the vector from the NH center of mass to the N atom. The radial grid R_i was from 2.5 to 10 Å in 0.25 Å steps and the angular grid θ_j was a set of 11 Gauss-Lobatto quadrature points, which include the two linear geometries. All interaction energies were corrected for basis-set superposition error using the counterpoise procedure [58].

Radial interpolation is carried out using the reproducing kernel Hilbert space (RKHS) method [59, 60] to evaluate

TABLE I. Basis-set dependence of the N–NH interaction energy at the global minimum for F12 calculations. The complete basis set (CBS) extrapolation was obtained with the correlation energy functional $E(X) = A + BX^{-3}$ [57] where X is the maximum angular momentum of electronic basis set.

basis set	$E_{\rm int}$ (cm^{-1})
aug-cc-pVTZ	−79.18
aug-cc-pVQZ	−86.03
aug-cc-pV5Z	−88.51
aug-cc-pV6Z	−89.33
CBS	−90.47
F12 /aug-cc-pVTZ	−89.10

TABLE II. Van der Waals coefficients for N–NH ($E_{\rm h} a_0^n$) from density-functional calculations.

n,λ	$C_{n,\lambda}$
6,0	33.50
6,2	11.44
7,1	60.87
7,3	55.28
8,0	717.14
8,2	988.87

$V(R,\theta_j)$ for arbitrary R and given θ_j. At each distance R, the potential is expanded in Legendre polynomials $P_\lambda(\cos\theta)$ for λ up to 8,

$$V(R,\theta) = \sum_\lambda V_\lambda(R) P_\lambda(\cos\theta). \quad (1)$$

The coefficients $V_\lambda(R)$ are obtained by integrating the *ab initio* potential using Gauss-Lobatto quadrature [35].

To provide an improved description of the long-range interaction, we impose an analytical representation on the long-range part of the components of the projected potential,

$$V_\lambda^{\rm lr}(R) = -\sum_{n=6}^{8}\sum_{\lambda=0}^{3} C_{n,\lambda} R^{-n}. \quad (2)$$

The Van der Waals coefficients are given in Table II and were calculated with the restricted open-shell coupled Kohn-Sham method [61] with asymptotically corrected [62] PBE0 functional [63]. We connect the long-range function smoothly to the supermolecular potential using the switching function [64]

$$f(R) = \frac{1}{2} + \frac{1}{4}\sin\frac{\pi x}{2}\left(3 - \sin^2\frac{\pi x}{2}\right), \quad (3)$$

where $x = \frac{R-b+R-a}{b-a}$ with $a = 7$ Å and $b = 11$ Å. $f(R) = 0$ for $R < 7$ Å and $f(R) = 1$ for $R > 11$ Å.

The potential energy surface for N–NH is shown in Fig. 1. It has two minima of comparable depths at linear geometries: 89.1 cm^{-1} at N–NH and 76.4 cm^{-1} at N–HN. The two minima are separated by a saddle point near the T-shaped geometry. The anisotropy of the potential near the Van der Waals minimum is about 40 cm^{-1}, and the dominant contribution to the anisotropy arises from $V_2(R)$.

TABLE III. Characteristic points on the N–NH potential energy surface. Energies are given in cm^{-1}, R in Å.

	Global minimum	Saddle point	Secondary minimum
R,θ	3.70,0	3.76, 92°	3.49, 180°
	−89.1	−39.2	−76.4

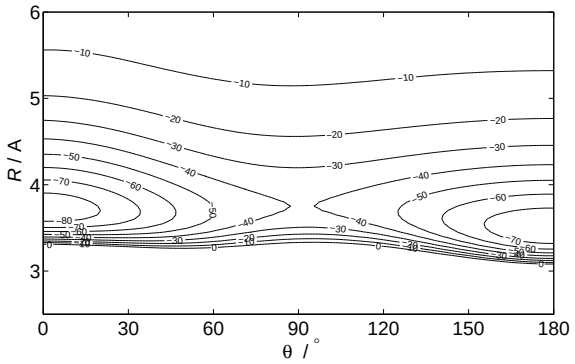

FIG. 1. The *ab initio* interaction potential of N–NH. Contours are labeled in cm^{-1}. The angle $\theta = 0$ corresponds to the N–N-H geometry.

1. Interaction potential uncertainty

An important problem in electronic structure theory is the estimation of error bounds for calculated interaction energies. Since scattering calculations at very low energies depend strongly on the details of the interaction, in this section we discuss the uncertainty of the N–NH interaction potential obtained here.

The largest contributions to the uncertainty of the interaction potential arise from the approximate treatment of electronic correlation and the incompleteness of the electronic basis set. We expect that the effect of the neglecting vibrations of the NH molecule is much less important, as are relativistic and nonadiabatic effects.

First we need to estimate how well the UCCSD(T) method works for sextet N–NH. To explore this, we performed 7-electron full configuration-interaction (FCI) calculations of the interaction energy. We included all electrons arising from the H atom and the $2p$ electrons of N atoms. With FCI it was possible to use only a very small basis set (6-31G, augmented with *spd* midbond functions with an exponent 0.4). For this small basis set, we compared the contribution to the correlation part of the interaction energy (i.e., the intramonomer correlation and the dispersion energy) with the UCCSD(T) results for several linear geometries N–NH and N–HN . The FCI correlation energy to be larger than the UCCSD(T) correlation energy by 1 to 1.5%, for a wide range of R and at both

linear geometries. To a good approximation we expect the *ratio* $E_{\rm corr}^{\rm FCI}/E_{\rm corr}^{\rm UCCSD(T)}$ to be constant in different basis sets. This suggests that the global minimum energy obtained with the coupled-cluster method is underestimated by ca. 1.5 cm^{-1}.

The basis set convergence pattern shown in Table I yields a complete basis-set limit of the global minimum depth of 90.47 cm^{-1}. This is 1.37 cm^{-1} more than in the method used for the complete surface here. We also performed test calculations including additional core-valence basis functions that are absent in the basis set used for the complete surface potential. The interaction energy at the global minimum obtained with aug-cc-pCVTZ is approximately 1 cm^{-1}*s*maller than for basis sets with no core-valence functions.

In summary we can set the error bounds on the interaction potential at the global minimum between -1 and +3 cm^{-1}, which is approximately between -1% and +3%.

III. N–NH SCATTERING CALCULATIONS

The Hamiltonian of the NH molecule may be written

$$H_{\rm NH} = b_{\rm NH}\hat{N}^2 + \gamma\hat{N}\cdot\hat{S} + \left[\frac{96\pi}{45}\right]^{\frac{1}{2}}\lambda_{\rm SS}\sum_q (-1)^q Y_{2,-q}(\hat{r})\,[S\otimes S]^{(2)}_q . \quad (4)$$

The three terms are, respectively, the rigid rotor Hamiltonian, the spin-rotation interaction and the intramonomer spin-spin interaction. The numerical values of the constants used in the present work are $b_{\rm NH} = 16.343$ cm^{-1} [65], $\gamma = -0.055$ cm^{-1} and $\lambda_{\rm SS} = 0.92$ cm^{-1} [66]. The NH molecule is assumed to be in its ground vibrational state.

The Hamiltonian of the N–NH collision system in a magnetic field may be written

$$H = -\frac{\hbar^2}{2\mu R}\frac{d^2}{dR^2}R + \frac{\hat{L}^2}{2\mu R^2} + H_{\rm NH} + H_{\rm Z} + V_{\rm SS} + V_{\rm int}(R,\theta). \quad (5)$$

Here $\hat{L}^2$ is the operator for the end-over-end angular momentum of N and NH about one another, H_Z represents the Zeeman interaction of N and NH with the magnetic field, $V_{\rm SS}$ is the (anisotropic) intermolecular spin-spin interaction, and $V_{\rm int}(R,\theta)$ is the intermolecular potential.

The convention for quantum numbers in this paper is as follows: L and M_L denote the end-over-end angular momentum and its projection onto the space-fixed Z axis defined by the magnetic field. Monomer quantum numbers are indicated with lower-case letters to avoid confusion with those of the collision system as a whole. The spins and spin projections of the N and NH molecules are denoted by $s_{\rm A}$, $s_{\rm B}$ and $m_{s\rm A}$, and $m_{s\rm B}$, respectively. The rotational quantum number of the NH molecule and its projection are denoted $n_{\rm B}$ and $m_{n\rm B}$ The projection of the total angular momentum,

$$M_{\rm tot} = M_L + m_{n\rm B} + m_{s\rm B} + m_{s\rm A}, \quad (6)$$

is rigorously conserved in a collision, but the total angular momentum itself is not, except at zero field. It is convenient to carry out scattering calculations is a fully uncoupled basis set, $|s_{\rm A}m_{s\rm A}\rangle|s_{\rm B}m_{s\rm B}\rangle|n_{\rm B}m_{n\rm B}\rangle|LM_L\rangle$. We have written a plug-in routine for the MOLSCAT scattering program [67], implementing all the matrix elements required for scattering calculations in this basis set.

The total spin S of a system made up of an open-shell atom and an open-shell molecule can take values between $|s_{\rm A}-s_{\rm B}|$ and $s_{\rm A}+s_{\rm B}$. For N–NH the allowed values are $S = \frac{1}{2}$, $\frac{3}{2}$ and $\frac{5}{2}$, corresponding to doublet, quartet and sextet, respectively. The interaction potential $V_{\rm int}(R,\theta)$ may be written in terms of projection operators,

$$V_{\rm int}(R,\theta) = \sum_{S=-|s_{\rm A}+s_{\rm B}|}^{s_{\rm A}+s_{\rm B}} |S\rangle V_S(R,\theta)\langle S| \quad (7)$$

and the general matrix element of $V_{\rm int}(R,\theta)$ in our basis set is

$$\langle s_{\rm A}m_{s\rm A}s_{\rm B}m_{s\rm B}n_{\rm B}m_{n\rm B}LM_L|V_{\rm int}(R,\theta)|s_{\rm A}m'_{s_{\rm A}}s_{\rm B}m'_{s\rm B}n'_{\rm B}m'_{n\rm B}L'M'_L\rangle = \sum_S (-1)^{2s_{\rm A}+2s_{\rm B}-m_{s\rm A}-m_{s\rm B}-M_L}(2S+1)\langle n_{\rm B}m_{n\rm B}LM_L|V_S(R,\theta)|n'_{\rm B}m'_{n\rm B}L'M'_L\rangle \begin{pmatrix} s_{\rm A} & s_{\rm B} & S \\ m_{s\rm A} & m_{s\rm B} & -m_{s\rm A}-m_{s\rm B}\end{pmatrix}\begin{pmatrix} s_{\rm A} & s_{\rm B} & S \\ m'_{s\rm A} & m'_{s\rm B} & -m'_{s\rm A}-m'_{s\rm B}\end{pmatrix}. \quad (8)$$

The three interaction potentials $V_S(R,\theta)$ differ only by short-range Pauli exchange terms. They have the same long-range coefficients, so become degenerate once the N atom and NH molecule are far enough apart that their valence shells do not overlap. The doublet surface has a potential well several hundred times deeper than the Van der Waals sextet state, so that full quantum calculations including the doublet state would require very large basis sets of rotational functions and could not be converged. In the present work we therefore approximate the operator $V_{\rm int}(R,\theta)$ operator by taking $V_S = V_{5/2}$ for all spin states. This approximation is legitimate because we are primarily interested in N–NH collisions between magnetically trapped atoms and molecules, with $m_{s\rm A} = s_{\rm A} = \frac{3}{2}$ and $m_{s\rm B} = s_{\rm B} = 1$. These are *spin-stretched* states, and $V_{3/2}$

and $V_{1/2}$ have no matrix elements (diagonal or off-diagonal) involving spin-stretched states. When this approximation is made, orthogonality relations for the $3j$ symbols reduce Eq. 8 to a form diagonal both in m_{sA} and m_{sB}. The explicit expression for $\langle n_B m_{nB} L M_L | V_S(R,\theta) | n_B m'_{nB} L' M'_L \rangle$ is the same as for scattering of NH from a closed-shell atom [5], with the addition of factors $\delta_{m_{sA} m'_{sA}}$.

The intermolecular spin-spin interaction has matrix elements

$$\begin{aligned}
&\langle s_A m_{sA} s_B m_{sB} n_B m_{nB} L M_L | V_{SS} | s_A m'_{sA} s_B m'_{sB} n'_B m'_{nB} L' M'_L \rangle = \\
&\sqrt{30}\lambda(R)\delta_{n_B n'_B}\delta_{m_{nB} m'_{nB}}(-1)^{s_A+s_B-m_{sA}-m_{sB}-M_L}[s_A(s_A+1)(2s_A+1)s_B(s_B+1)(2s_B+1)(2L+1)(2L'+1)]^{\frac{1}{2}} \\
&\begin{pmatrix} L & 2 & L' \\ 0 & 0 & 0 \end{pmatrix} \sum_{q_1 q_2} \begin{pmatrix} L & 2 & L' \\ -M_L & -q_1-q_2 & M'_L \end{pmatrix} \begin{pmatrix} 1 & 1 & 2 \\ q_1 & q_2 & -q_1-q_2 \end{pmatrix} \\
&\begin{pmatrix} s_A & 1 & s_A \\ -m_{sA} & q_1 & m'_{sA} \end{pmatrix} \begin{pmatrix} s_B & 1 & s_B \\ -m_{sB} & q_2 & m'_{sB} \end{pmatrix}. \qquad (9)
\end{aligned}$$

The spin-spin coupling constant $\lambda(R)$ is $E_h \alpha^2 a_0^3/R^3$, where E_h is the Hartree energy and α is the fine-structure constant.

The matrix elements for NH monomer operators are the same as for scattering of NH from a closed-shell atom [5], with the addition of factors $\delta_{m_{sA} m'_{sA}}$.

If one or both of the colliding species is not in a spin-stretched state (with the highest possible value of m_S), the system will undergo very fast spin exchange driven by the *difference* between the $S = \frac{5}{2}$, $\frac{3}{2}$ and $S = \frac{1}{2}$ potentials. For spin-stretched states, however, spin exchange cannot occur and only spin relaxation is possible. There are two mechanisms for spin relaxation. The first is similar to the well-known mechanism of spin relaxation for spin-stretched states of alkali metal atoms, and arises through direct coupling of the initial state $m_{sA} = +\frac{3}{2}, m_{sB} = +1$ (with $n_B = m_{nB} = 0$), to final states with m_{sA} and/or m_{sB} reduced by 1 by the intermolecular spin-spin interaction term and M_L increased to conserve M_{tot}. Such transitions are relatively slow, because the intermolecular spin-spin interaction is weak. The second mechanism is that described by Krems and Dalgarno [68]. For the same initial state, the intramonomer spin-spin interaction mixes $n_B = 0$ with $n_B = 2$, and even in a magnetic field it mixes $m_{nB} = 0$ with $m_{nB} = \pm 1, \pm 2$. The states with $m_{nB} = +1, +2$ have $m_{sB} = 0, -1$. The states with $m_n = 1, 2$ are then coupled by the anisotropy of the interaction potential to $n = 0$, $m_n = 0$ states with changed M_L but the same m_B (which is lower than in the initial state). This mechanism is also expected to be fairly weak for a low-anisotropy system such as N–NH: the $n = 0$ and $n = 2$ rotational levels of NH differ in energy by 96 cm^{-1}, while the potential anisotropy $V_2(R)$ that couples them is a short-range interaction that is never greater than 40 cm^{-1} in the energetically accessible region. For both mechanisms, spin relaxation is suppressed for s-wave scattering ($L = 0, M_L = 0$) at low energies and fields because the conservation of M_{tot} requires $M'_L \neq 0$ and therefore $L' > 0$, producing a centrifugal barrier in the outgoing channel.

We carry out scattering calculations with the MOLSCAT package [67]. The coupled equations are solved using the hybrid log-derivative/Airy propagator of Alexander and Manolopoulos [69]. We used the fixed-step log-derivative propagator from 2.8 Å to 70 Å with an interval size of 0.08 Å, followed by a variable-step Airy propagation out to 400 Å. We carried out convergence tests on state-to-state cross sections both in the s-wave regime and at energies up to $E = 1$ K, at fields of $B = 200$ G, 1000 G and 2 T. In all cases a basis set with $n = 0 \ldots 3$ and $L = 0 \ldots 7$ gave convergence to within approximately 1% for all state-to-state cross sections. This basis set was therefore used in all the remaining calculations.

IV. RESULTS

Fig. 2 shows the Zeeman energy levels of the noninteracting N+NH system. In the buffer-gas cooling experiment, [43] both atoms and molecules are trapped in their low-field-seeking state with $m_{sA} = \frac{3}{2}$ and $n_B = m_{nB} = 0$, $m_{sB} = 1$. The experiment has already achieved temperatures around 550 mK, and at this temperature atoms with an energy of $5kT$ sample magnetic fields up to 2 T in a quadrupole trap. However, as the temperature decreases, so too will the magnetic fields sampled. We therefore consider collision energies from 10 μK to 1 K and fields from 10 G to 2 T.

The N atom is considerably less polarizable than alkali metal or alkaline earth atoms. As a result, the dispersion coefficient $C_{6,0}$ for N–NH is considerably lower than for most metal atom – molecule systems that have been considered previously as candidates for sympathetic cooling. Together with a low reduced mass, this results in relatively high centrifugal barriers for $L > 0$ partial waves: 14 mK for $L = 1$, 71 mK for $L = 2$, 120 mK for $L = 3$, etc. The high centrifugal barriers also mean that quite small number of partial waves are needed to converge cross sections: for example, including contributions from L up to 4 is sufficient to obtain convergence up to about 0.5 K.

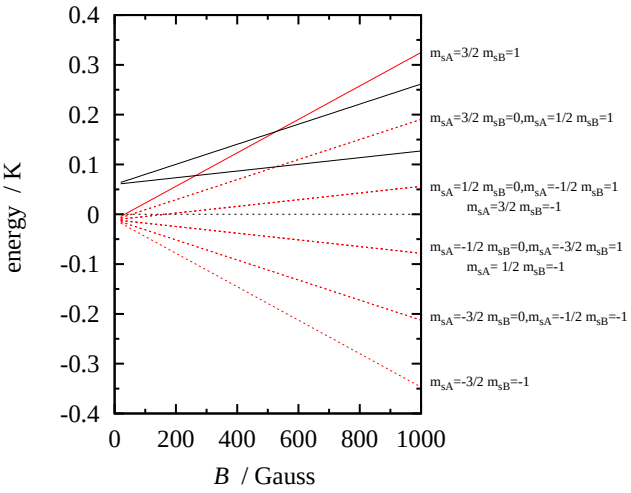

FIG. 2. Energy levels of the noninteracting N+NH system in a magnetic field. The dotted red lines show the energy obtained by adding the d-wave centrifugal barrier height (71 mK) to the levels with $M_{\rm tot} = \frac{3}{2}$ and $M_{\rm tot} = \frac{1}{2}$. The crossings between the red lines and the initial-state energy indicate the fields above which s-wave inelastic cross sections are no longer suppressed by centrifugal barriers.

A. Close-coupling calculations

Calculated elastic and inelastic cross sections for the four different isotopic combinations are shown as a function of collision energy E in Fig. 3, for representative magnetic fields of 200 G, 300 G, 1000 G and 2 T. In a simple hard-sphere model of sympathetic cooling, neglecting inelastic collisions, the temperature relaxes towards equilibrium and reaches a $1/e$ point after $(m_1+m_2)^2/2m_1m_2$ collisions [70], where m_1 and m_2 are the masses of the two species. For sympathetic cooling to be successful we need the ratio of elastic to inelastic cross sections to be much larger than this. The calculated ratios are shown in Fig. 4: for the most part they are more than 50 at collision energies above about 1 mK, indicating that sympathetic cooling of NH by N is likely to be feasible.

Several different effects are evident in Fig. 3. The first is that the cross sections enter the s-wave regime, where they are proportional to $E^{-1/2}$, at quite different energies for different isotopic species. This occurs because of p-wave resonant effects. Once in the s-wave regime, however, the inelastic cross sections generally decrease at magnetic fields below about 300 G, because of the centrifugal barriers in the outgoing channels. Since atoms and molecules in a quadrupole trap sample lower and lower fields as the temperature is decreased, this indicates that sympathetic cooling will become increasingly effective as the temperature is lowered, as predicted for Mg-NH [37]. Lastly, inelastic collisions are also suppressed for very *high* magnetic fields. All these effects will be discussed in more detail below.

Spin relaxation collisions can change $m_{s\rm A}$ for the N atom, $m_{s\rm B}$ for the NH molecule, or both. Fig. 5 shows the state-to-state cross sections for the most important final states for ^{15}N–^{15}NH as a function of energy at two different fields. It may be

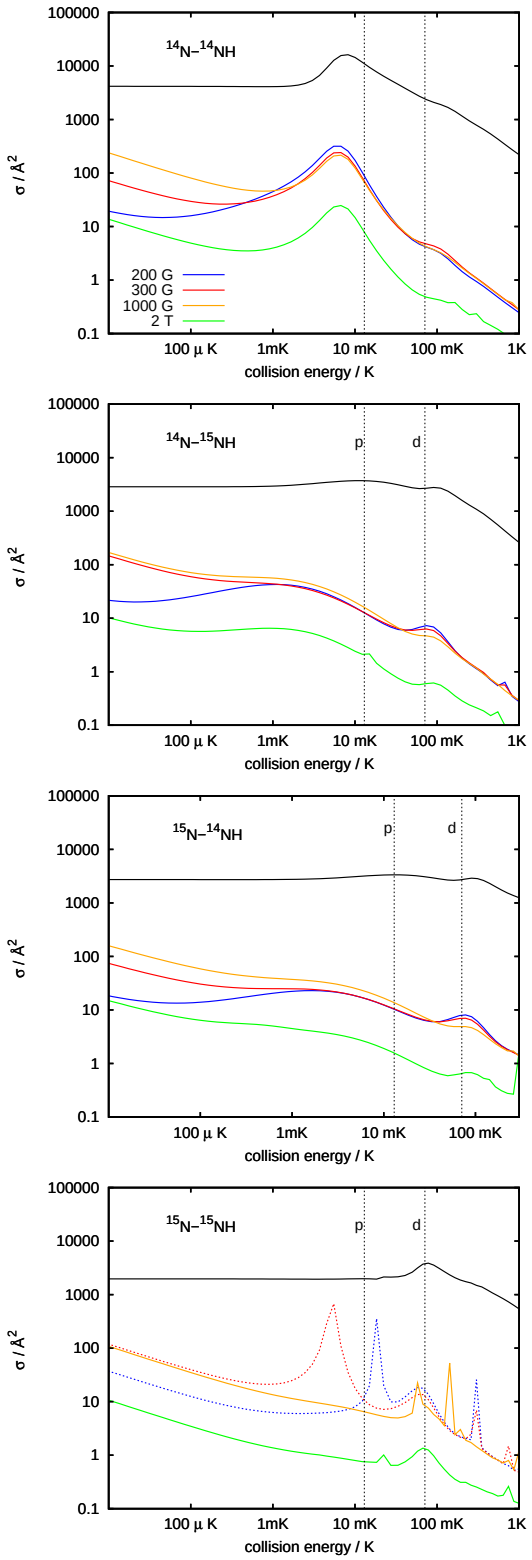

FIG. 3. Elastic and inelastic cross sections for N–NH scattering for ^{14}N–^{14}NH, ^{14}N–^{15}NH, ^{15}N–^{14}NH and ^{15}N–^{15}NH for different magnetic fields. The elastic cross section (black line) is almost independent of field. The positions of the p- and d-wave exit-channel barriers are marked with vertical lines.

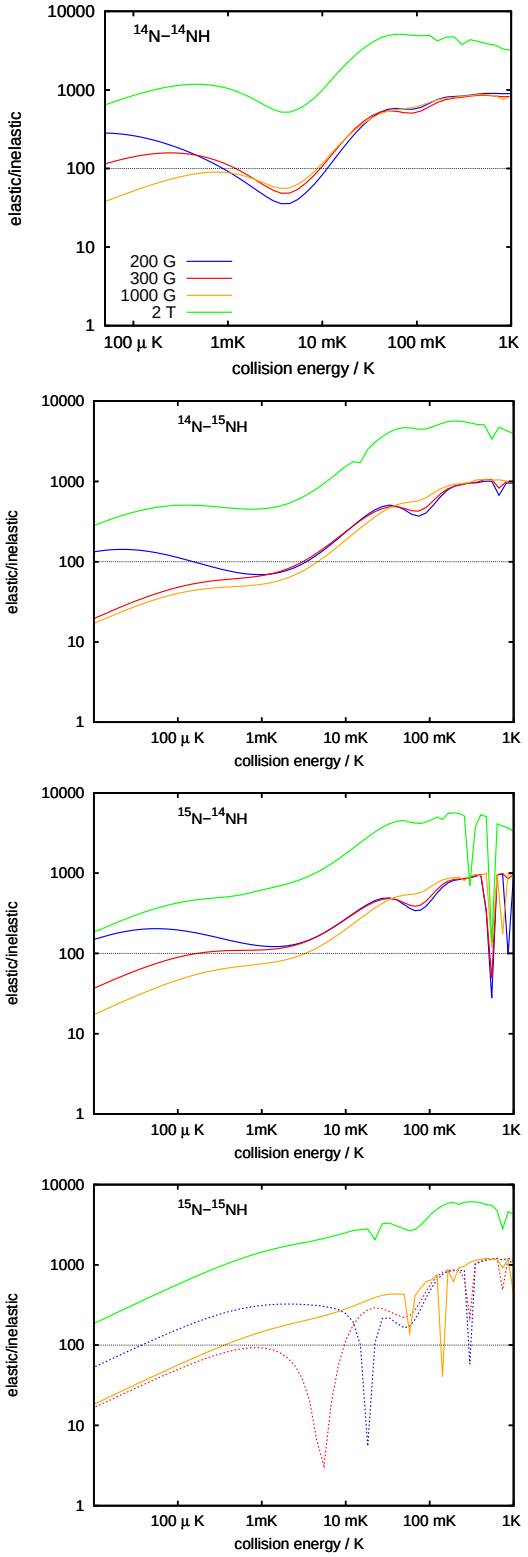

FIG. 4. The ratio of elastic to inelastic cross sections for ^{14}N – ^{14}NH, ^{14}N – ^{15}NH, ^{15}N – ^{14}NH and ^{15}N – ^{15}NH systems for different magnetic fields. The value of 100 typically required for sympathetic cooling is marked with a dotted horizontal line.

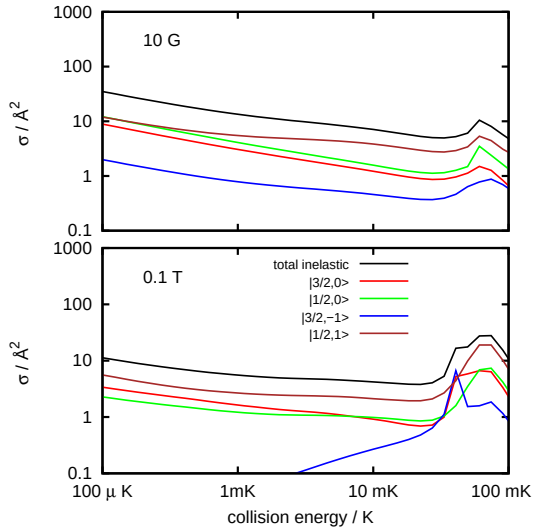

FIG. 5. State-to-state inelastic cross sections for ^{15}N – ^{15}NH for weak (10 G) and strong (0.1 T) magnetic fields.

seen that dominant final states are those in which m_{sA} and/or m_{sB} has changed by 1. These collisions are driven by the intermolecular spin-spin interaction. Transitions that change m_{sB} by 2 can occur only by the second mechanism described in Section III above, involving the potential anisotropy, and are seen to be very much weaker except in a small resonant region.

The ^{14}N–^{14}NH system shows behaviour quite different from the others, with a large peak in the inelastic cross sections near 10 mK which reduces the elastic-to-inelastic ratio to around 10. This ratio may not be high enough for effective sympathetic cooling from an initial temperature of tens of milliKelvin. The peak appears at the same energy for all values of the field. It arises from a p-wave shape resonance in the incoming channel, as discussed in section IV C below. For the larger reduced masses of the other isotopic combinations, the quasibound state responsible for the shape resonance drops below threshold and becomes a true bound state. Thus the other isotopic combinations do not exhibit this feature and have more favourable properties for sympathetic cooling.

The ^{15}N–^{15}NH system exhibits d-wave shape resonances for collision energies of 50 to 70 mK, but they are much weaker than the p-wave resonance for ^{14}N–^{14}NH and their presence does not strongly affect the total inelastic cross section.

The $L = 2$ centrifugal barrier plays a crucial role in spin relaxation in the ultracold regime. For an incoming channel with $L = 0$, spin relaxation requires outgoing $L \geq 2$. If the energy difference between the incoming and outgoing channels is smaller than the height of the $L = 2$ centrifugal barrier, the s-wave inelastic cross section is suppressed (see Fig. 2). The s-wave state-to-state cross sections are shown as a function of magnetic field in Fig. 6 for ^{14}N–^{14}NH at a collision energy of 50 μK. The inelastic cross sections generally decrease at magnetic fields below about 500 G, though there is a dip in

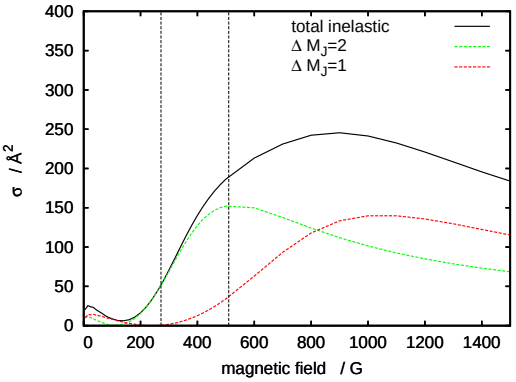

FIG. 6. Inelastic s-wave cross section as a function of magnetic field for ^{14}N–^{14}NH at a collision energy of 50 μK. The dashed vertical lines correspond to the fields for which the kinetic energy release from $M_{\rm tot} = \frac{5}{2}$ to $M_{\rm tot} = \frac{3}{2}$ and $M_{\rm tot} = \frac{1}{2}$ states are equal to the height of the d-wave barrier.

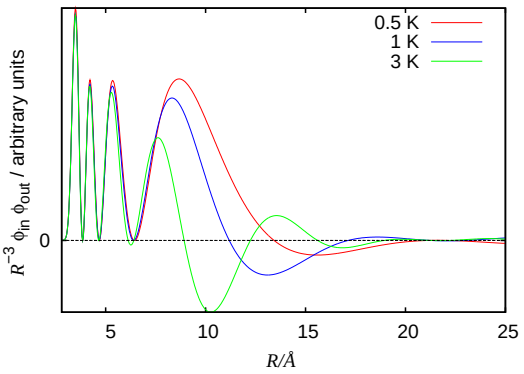

FIG. 7. The integrand of the distorted-wave Born approximation (Eq. 10) for ^{14}N–^{14}NH at a collision energy of 1 mK for different kinetic energy releases. The incoming wavefunction is calculated for $L = 0$ and the outgoing wavefunction for $L = 2$.

each state-to-state component between 100 and 300 G. These dips are due to suppression of the inelastic cross sections in the wings of resonances, as described by Hutson *et al.* [6]; in this case the resonances concerned are shape resonances in the d-wave outgoing channels.

The suppression of inelastic scattering by the centrifugal barrier is clear in the total inelastic cross section only for systems with reduced mass larger than for ^{14}N–^{14}NH. For the ^{14}N–^{14}NH system itself, the p-wave contribution is very strong even at very low energies. In fact, the p-wave enhancement of the inelastic cross section between 50 μK and 1 mK is so strong that the total inelastic cross section does not follow the $E^{-\frac{1}{2}}$ power-law dependence expected from the Wigner threshold laws at these energies.

Suppression of inelastic collisions due to barriers in the outgoing channels decreases as the magnetic field increases (so that the kinetic energy release increases). Eventually, however, the inelastic cross section reaches a maximum and starts to decrease again. This occurs for all partial waves, and the total cross sections at a field of 2 T are typically reduced by a factor of about 10 from their values at 0.1 T. Since for some isotopic combinations the low-field ratio of elastic to inelastic cross sections may not be large enough at temperatures of 1 to 10 mK, the application of a strong bias field to a magnetic trap offers a possible way way to improve the ratio.

Suppression of inelastic cross sections at high fields has been observed for O(^{3}P)-He collisions [71], for OH-OH [72] and for collisions of Cr atoms [73]. For small inelasticity, the distorted-wave Born approximation gives [74]

$$\sigma_{i\to f} = 4\pi k_i^{-2} \left| \int \psi_i(R) U_{if}(R) \psi_f(R)\, dR \right|^2, \qquad (10)$$

where ψ_i and ψ_f are energy-normalized wavefunctions in the initial and final channels, U_{if} is the coupling between the channels, and k_i is the wave vector in the incoming channel. Fig. 7 shows the integrand of Eq. 10 for the intermolecular spin-spin term (R^{-3}) at kinetic energy releases of 0.5 K, 1 K and 3 K, corresponding to fields of 3800 G, 7600 G and 2.3 T for transitions with $\Delta m_{s\rm A} + \Delta m_{s\rm B} = -1$. It may be seen that there is significant oscillatory cancellation in the integral at high fields, when $\psi_i(R)$ and $\psi_f(R)$ oscillate out of phase with one another in the interaction region, and this combines with the effect of the resonances in the d-wave outgoing channels to produce the maxima in Fig. 6. The oscillatory cancellation occurs for arbitrary partial waves.

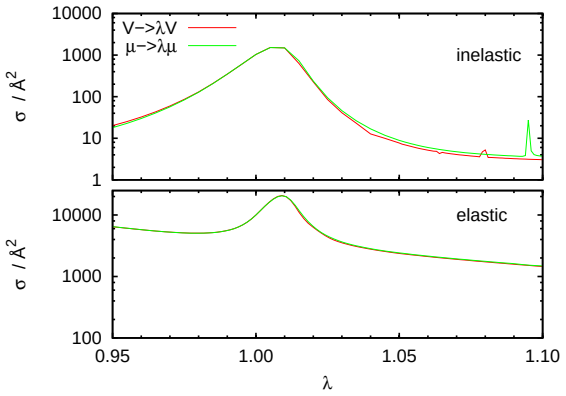

FIG. 8. Elastic and total inelastic cross sections for ^{14}N–^{14}NH at $E = 5$ mK and $B = 50$ G as a function of both reduced mass and potential scaling factors.

B. Dependence on interaction potential and reduced mass

Because of the crucial role played by the p-wave shape resonance for ^{14}N–^{14}NH at energies up to 10 mK, it is important to investigate the influence of uncertainties in the interaction potential on the cross sections. The shape of the 2D interaction potential is complicated and the scattering properties might in principle depend on many parameters. However, Gribakin and Flambaum [75] showed that for single-channel

scattering the scattering length a behaves as

$$a = \bar{a}\left[1 - \tan\left(\Phi - \frac{\pi}{8}\right)\right], \tag{11}$$

where, for a potential with long-range form $-C_6R^{-6}$, the mean scattering length $\bar{a}$ is $0.956(2\mu C_6/\hbar^2)^{\frac{1}{4}}$ and

$$\Phi = \int_0^\infty \left(2\mu V_{\rm int}(R)/\hbar^2\right)^{\frac{1}{2}} dR. \tag{12}$$

Although N–NH is a many-channel scattering problem, it is elastically dominated and Eq. 12 with $V_{\rm int}(R)$ replaced by $V_0(R)$ reproduces the major features of the elastic scattering. Thus scaling μ is approximately equivalent to scaling the entire interaction potential, and either of these scalings provides a good way to explore the variation of scattering length as a function of potential. Fig. 8 shows the elastic and total inelastic cross sections for ^{14}N–^{14}NH at $E = 5$ mK and $B = 50$ G as a function of both reduced mass and potential scaling factors. It may be seen that the two scalings have a very similar effect, apart from a small shift in the Feshbach resonance around $\lambda = 1.08$, which comes from a rotationally excited state of NH.

We estimate the bounds on the accuracy of our potential to be between -2.5 and $+3\%$ of the well depth. We have therefore carried out calculations of the cross sections as a function of a variable reduced mass, parameterized by scaling factor $\mu \to \lambda\mu$ for a collision energy of 5 mK. A scaling factor $\lambda = 1$ corresponds to the reduced mass for ^{14}N–^{14}NH. The result is shown in Fig. 9. There is a strong maximum in the total inelastic cross section near $\lambda = 1.012$, due to a p-wave shape resonance in the *elastic* channel. A change of 1.2% in the potential is within the estimated error bound of our calculations. Enhancement of the cross sections due to the p-wave resonance might thus occur for heavier isotopic combinations than ^{14}N–^{14}NH if our potential is slightly too deep. Although we believe it is more likely that our potential is too shallow than too deep, this cannot be ruled out. However, it is quite unlikely that enhancement due to the p-wave resonance would occur for the heaviest system, ^{15}N–^{15}NH.

C. AQDT analysis of shape resonances

In this section we consider the N–NH scattering in the context of angular-momentum-insensitive quantum defect theory (AQDT) [47]. The upper part of Fig. 10 shows the positions of (quasi)bound states for $L = 0 \ldots 2$ as a function of the reduced-mass scaling factor λ for values between 0.8 and 1.2. The $L = 0$ bound state crosses the threshold at a value of the reduced mass much smaller than that for ^{14}N–^{14}NH, well outside the estimated error bounds for the potential. There is thus no s-wave resonance in the scattering for any of the systems considered here.

The p-wave shape resonance in the cross sections for ^{14}N–^{14}NH arises from the quasibound state with $L = 1$, which is 6 mK above threshold for $\lambda = 1$. As the reduced mass increases above this, the $L = 1$ bound state crosses the threshold at $\lambda =$

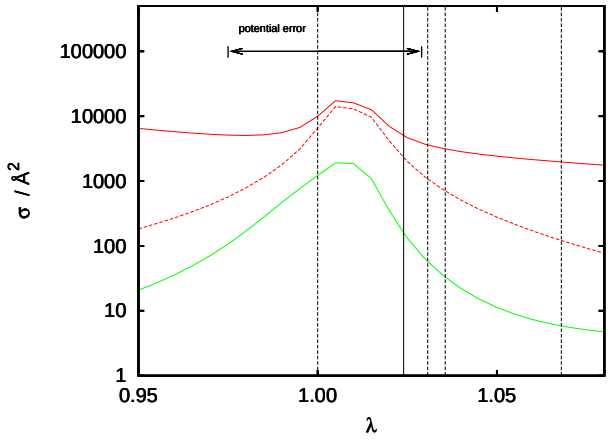

FIG. 9. Elastic and inelastic cross sections for a collision energy of 5 mK as a function of scaled reduced mass. The dashed vertical lines indicate the values of μ for the systems concerned here, from left to right, ^{14}N–^{14}NH, ^{14}N–^{15}NH, ^{15}N–^{14}NH and ^{15}N–^{15}NH, respectively. The solid vertical line shows the value $\lambda = 1.024$ for which the scattering length $a = 2\bar{a}$.

1.024 and becomes a "real" bound state. This explains why we see no p-wave shape resonances in the cross sections for collisions with reduced mass larger than $1.024\mu_{14,14}$, i.e. for all systems containing at least one ^{15}N atom. For large values of μ the $L = 2$ bound state comes close to threshold, and this results in the (small) d-wave shape resonance that can be seen in the ^{15}N–^{15}NH cross sections.

The lower panel of Fig. 10 shows the s-wave scattering length as a function of scaling factor λ. As expected, there is a pole near $\lambda = 0.9$ as the $L = 0$ bound state crosses the threshold. Within the estimated error bounds of the potential, a varies between 22.3 and 15.2 Å, so that the elastic cross section for small $E_{\rm coll}$ (in the Wigner regime) varies between 6250 and 2900 Å^2.

In angular-momentum-insensitive quantum defect theory [47, 76, 77], the scattering properties of a system for arbitrary L can be predicted from only a few parameters: the s-wave scattering length a, the dispersion coefficient C_6 and the reduced mass μ (and thus $\bar{a}$). The positions where $L > 0$ bound states cross threshold, and hence produce shape resonances, depend only on the relationship between a and $\bar{a}$. In particular, when $a = 2\bar{a}$ there is an $L = 1$ bound state exactly at threshold, and systems with a slightly larger than $2\bar{a}$ have a p-wave shape resonance at a collision energies below the height of the p-wave centrifugal barrier. This is the case for the ^{14}N–^{14}NH system here. For $a = \bar{a}$ there is an $L = 2$ bound state exactly at threshold. The scattering length for ^{15}N–^{15}NH is $1.54\bar{a}$, which is close enough above $\bar{a}$ to produce a d-wave shape resonance at finite energy. The energies at which the p-wave and d-wave resonances appear can be read off the $L = 1$ and 2 lines in Fig. 10.

It should be noted that a change in the interaction potential would result in “sliding" the vertical lines representing the four isotopic combinations horizontally along Fig. 10. A range of behaviour can exist for potentials within our un-

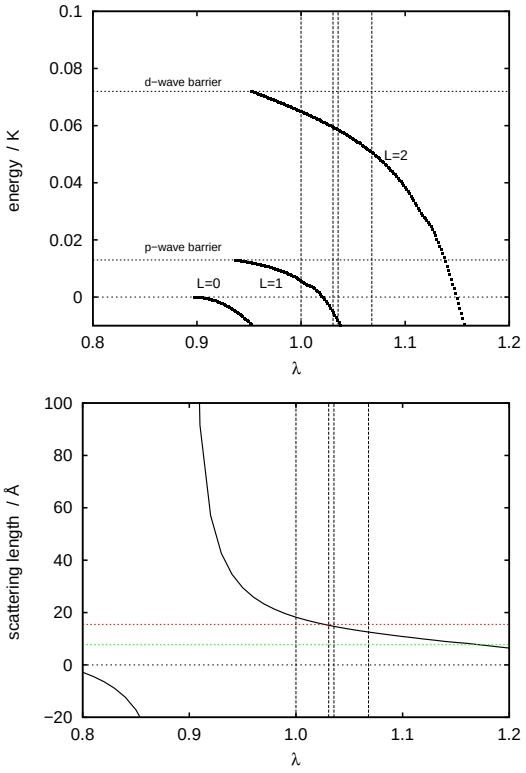

FIG. 10. Near-threshold bound states of sextet N–NH for $L = 0 \ldots 2$ as a function of μ (upper panel), and the μ-dependence of the s-wave scattering length (lower panel). Field-free calculations with a structureless atom and diatom were used to obtain the bound states here. The dashed vertical lines indicate the values of μ for ^{14}N–^{14}NH, ^{14}N–^{15}NH, ^{15}N–^{14}NH and ^{15}N–^{15}NH, respectively, from left to right. The red dotted line on the lower panel indicates $2\bar{a}$ and the green dotted line indicates $\bar{a}$.

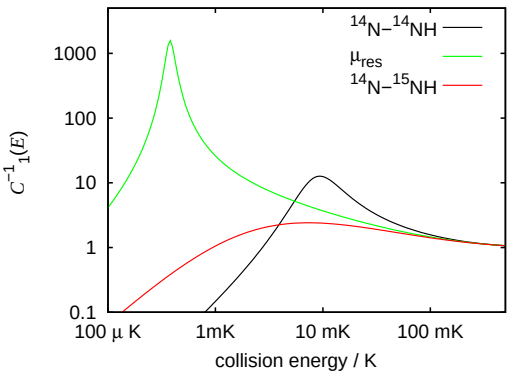

FIG. 11. The p-wave transmission function $C_1^{-1}(E)$ for N–NH systems with reduced masses corresponding to: ^{14}N–^{14}NH ($a/\bar{a} = 2.34$), ^{14}N–^{15}NH ($a/\bar{a} = 1.94$), and an artificial system with $\lambda = 1.031$, for which $a/\bar{a} \to 2^+$.

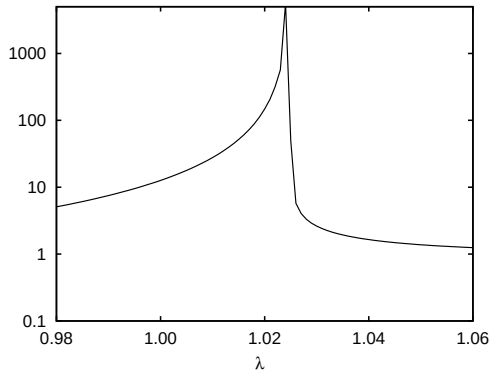

FIG. 12. The height of the peak in the $C_1^{-1}(E)$ function as a function of reduced-mass scaling factor λ.

certainties of our calculations. Our calculations thus do not definitively identify which characteristics will be be observed for a particular isotopic combination.

To study the shape of the resonant features more quantitatively, we can consider the $C_L(E)$ functions introduced by Mies [78, 79]. These functions give the connection between a semiclassical JWKB description of scattering states (valid at large collision energies) and the near-threshold behaviour. The function $C_L^{-1}(E)$ can be viewed as an enhancement factor in the short-range part of the wavefunction due to the presence of the long-range potential, including any resonant effects in the incoming channel. In Fig. 11 we show the $C_1^{-1}(E)$ functions for p-wave scattering with $\lambda = 1$, 1.023 and 1.031 (the last of these values corresponding to the reduced mass of ^{14}N–^{15}NH). As the scattering length decreases and reaches $2\bar{a}$, the height of the peak in $C_1^{-1}(E)$ goes to $+\infty$, as shown in Fig. 12, and the energy at which the peak occurs approaches zero. The width of the resonance decreases, corresponding to increasing the lifetime of the quasibound state. The intensity of the resonance rapidly decreases once the scattering length is larger than $2\bar{a}$, corresponding to a bound state below threshold.

V. CONCLUSIONS

We have calculated a potential energy surface for N atoms (^4S) interacting with NH molecules ($^3\Sigma^-$) in the spin-$\frac{5}{2}$ (sextet) state, using unrestricted coupled-cluster calculations with an explicitly correlated basis set. This is the surface that governs collisions of cold N atoms and NH molecules in a magnetic trap. We have used the surface to carry out quantum scattering calculations of cold collisions for different isotopic combinations of N and NH, as a function of collision energy and magnetic field.

The sextet potential energy surface is weakly anisotropic, with an anisotropy of approximately 40 cm^{-1} in the well region. The anisotropy is dominated by the $P_2(\cos\theta)$ Legendre, which mixes states with $\Delta n = \pm 2$ in the NH rotational quantum n. Since the anisotropy is smaller than the separation between the $n = 0$ and 2 states, it causes relatively weak mixing during collisions and the scattering is generally elastically dominated. The inelastic cross sections are suppressed both at low energy and low field (by centrifugal barrier in the exit channels) and at very high field (by oscillatory cancellation due to the large kinetic energy release). For most isotopic

combinations the ratio of elastic to inelastic cross sections is high enough, over a wide enough range of collision energy and magnetic field, that sympathetic cooling of NH by N is a good prospect.

We have shown that a scaling of the interaction potential is approximately equivalent in its effects to a scaling of the collision reduced mass. We estimate our interaction potential to be accurate to within 3%. We have investigated scaling the reduced mass by up to 20% from the value for ^{14}N–^{14}NH. The scaling revealed that there are major effects arising for a p-wave shape resonance, which produce enhanced inelastic scattering for ^{14}N–^{14}NH at low energies on our best potential surface. We have used angular-momentum-insensitive quantum defect theory (AQDT) to understand how the results change for different isotopic combinations.

Scaling the potential energy surface, or equivalently the reduced mass, is a very useful tool for understanding cold collision calculations. In combination with AQDT, it can provide powerful insights into low-energy scattering for low-energy collisions where where only a few partial waves contribute to the scattering.

ACKNOWLEDGMENTS

We are grateful to John Doyle for interesting us in this problem, and to Alisdair Wallis for valuable discussions. This work is supported by EPSRC under collaborative project CoPoMol of the ESF EUROCORES Programme EuroQUAM.

[1] E. P. Wigner, *Phys. Rev.*, 1948, **73**, 1002–1009.
[2] N. Balakrishnan, R. C. Forrey and A. Dalgarno, *Chem. Phys. Lett.*, 1997, **280**, 1–4.
[3] R. C. Forrey, N. Balakrishnan, V. Kharchenko and A. Dalgarno, *Phys. Rev. A*, 1998, **58**, R2645–R2647.
[4] R. V. Krems, *Int. Rev. Phys. Chem.*, 2005, **24**, 99–118.
[5] M. L. González-Martínez and J. M. Hutson, *Phys. Rev. A*, 2007, **75**, 022702.
[6] J. M. Hutson, M. Beyene and M. L. González-Martínez, *Phys. Rev. Lett.*, 2009, **103**, 163201.
[7] J. M. Sage, S. Sainis, T. Bergeman and D. DeMille, *Phys. Rev. Lett.*, 2005, **94**, 203001.
[8] J. Deiglmayr, A. Grochola, M. Repp, K. Mörtlbauer, C. Glück, J. Lange, O. Dulieu, R. Wester and M. Weidemüller, *Phys. Rev. Lett.*, 2008, **101**, 133004.
[9] M. Viteau, A. Chotia, M. Allegrini, N. Bouloufa, O. Dulieu, D. Comparat and P. Pillet, *Science*, 2008, **321**, 232.
[10] K.-K. Ni, S. Ospelkaus, M. H. G. de Miranda, A. Pe'er, B. Neyenhuis, J. J. Zirbel, S. Kotochigova, P. S. Julienne, D. S. Jin and J. Ye, *Science*, 2008, **322**, 231.
[11] J. G. Danzl, M. J. Mark, E. Haller, M. Gustavsson, R. Hart, J. Aldegunde, J. M. Hutson and H.-C. Nägerl, *Nature Physics*, 2010, **6**, 265–270.
[12] J. Aldegunde, B. A. Rivington, P. S. Żuchowski and J. M. Hutson, *Phys. Rev. A*, 2008, **78**, 033434.
[13] J. Aldegunde and J. M. Hutson, *Phys. Rev. A*, 2009, **79**, 013401.
[14] J. Aldegunde, H. Ran and J. M. Hutson, *Phys. Rev. A*, 2009, **80**, 043410.
[15] S. Ospelkaus, K.-K. Ni, D. Wang, M. H. G. de Miranda, B. Neyenhuis, G. Quéméner, P. S. Julienne, J. L. Bohn, D. S. Jin and J. Ye, *Science*, 2010, **327**, 853–857.
[16] J. M. Hutson, *Science*, 2010, **327**, 788–789.
[17] H. L. Bethlem, G. Berden and G. Meijer, *Phys. Rev. Lett.*, 1999, **83**, 1558–1561.
[18] J. D. Weinstein, R. deCarvalho, T. Guillet, B. Friedrich and J. M. Doyle, *Nature*, 1998, **395**, 148–150.
[19] D. Egorov, T. Lahaye, W. Schollkopf, B. Friedrich and J. M. Doyle, *Phys. Rev. A*, 2002, **66**, 043401.
[20] M. S. Elioff, J. J. Valentini and D. W. Chandler, *Science*, 2003, **302**, 1940–1943.
[21] T. Junglen, T. Rieger, S. A. Rangwala, P. W. H. Pinkse and G. Rempe, *Eur. Phys. J. D*, 2004, **31**, 365–373.
[22] K. Maussang, D. Egorov, J. S. Helton, S. V. Nguyen and J. M. Doyle, *Phys. Rev. Lett.*, 2005, **94**, 123002.
[23] D. Egorov, W. C. Campbell, B. Friedrich, S. E. Maxwell, E. Tsikata, L. D. van Buuren and J. M. Doyle, *Eur. Phys. J. D*, 2004, **31**, 307–311.
[24] W. C. Campbell, E. Tsikata, H.-I. Lu, L. D. van Buuren and J. M. Doyle, *Phys. Rev. Lett.*, 2007, **98**, 213001.
[25] M. Stoll, J. M. Bakker, T. C. Steimle, G. Meijer and A. Peters, *Phys. Rev. A*, 2008, **78**, 032707.
[26] J. Kim, B. Friedrich, D. P. Katz, D. Patterson, J. D. Weinstein, R. DeCarvalho and J. M. Doyle, *Phys. Rev. Lett.*, 1997, **78**, 3665–3668.
[27] J. D. Weinstein, R. deCarvalho, C. I. Hancox and J. M. Doyle, *Phys. Rev. A*, 2002, **65**, 021604.
[28] C. I. Hancox, M. T. Hummon, S. V. Nguyen and J. M. Doyle, *Phys. Rev. A*, 2005, **71**, 031402.
[29] S. C. Doret, C. B. Connolly, W. Ketterle and J. M. Doyle, *Phys. Rev. Lett.*, 2009, **103**, 103005.
[30] D. J. Larson, J. C. Bergquist, J. J. Bollinger, W. M. Itano and D. J. Wineland, *Phys. Rev. Lett.*, 1986, **57**, 70–73.
[31] A. Ostendorf, C. B. Zhang, M. A. Wilson, D. Offenberg, B. Roth and S. Schiller, *Phys. Rev. Lett.*, 2006, **97**, 243005.
[32] G. Modugno, G. Ferrari, G. Roati, R. J. Brecha, A. Simoni and M. Inguscio, *Science*, 2001, **294**, 1320–1322.
[33] P. Soldán and J. M. Hutson, *Phys. Rev. Lett.*, 2004, **92**, 163202.
[34] M. Lara, J. L. Bohn, D. Potter, P. Soldán and J. M. Hutson, *Phys. Rev. Lett.*, 2006, **97**, 183201.
[35] M. Lara, J. L. Bohn, D. E. Potter, P. Soldán and J. M. Hutson, *Phys. Rev. A*, 2007, **75**, 012704.
[36] P. Soldán, P. S. Żuchowski and J. M. Hutson, *Faraday Discuss.*, 2009, **142**, 191.
[37] A. O. G. Wallis and J. M. Hutson, *Phys. Rev. Lett.*, 2009, **103**, 183201.
[38] H. L. Bethlem, F. M. H. Crompvoets, R. T. Jongma, S. Y. T. van de Meerakker and G. Meijer, *Phys. Rev. A*, 2002, **65**, 053416.
[39] P. S. Żuchowski and J. M. Hutson, *Phys. Rev. A*, 2008, **78**, 022701.
[40] P. S. Żuchowski and J. M. Hutson, *Phys. Rev. A*, 2009, **79**, 062708.
[41] H. L. Bethlem, G. Berden, F. M. H. Crompvoets, R. T. Jongma, A. J. A. van Roij and G. Meijer, *Nature*, 2000, **406**, 491–494.
[42] J. van Veldhoven, H. L. Bethlem and G. Meijer, *Phys. Rev. Lett.*, 2005, **94**, 083001.

[43] M. T. Hummon, W. C. Campbell, H.-I. Lu, E. Tsikata, Y. Wang and J. M. Doyle, *Phys. Rev. A*, 2008, **78**, 050702.

[44] T. V. Tscherbul, J. Kłos, A. Dalgarno, B. Zygelman, Z. Pavlovic, M. T. Hummon, H.-I. Lu, E. Tsikata and J. M. Doyle, *arXiv:1007.0469*, 2010.

[45] S. V. Nguyen, S. C. Doret, C. B. Connolly, R. A. Michniak, W. Ketterle and J. M. Doyle, *Phys. Rev. A*, 2005, **72**, 060703.

[46] S. V. Nguyen, R. deCarvalho and J. M. Doyle, *Phys. Rev. A*, 2007, **75**, 062706.

[47] B. Gao, *Phys. Rev. A*, 2001, **64**, 010701.

[48] L. A. Poveda and A. J. C. Varandas, *J. Phys Chem. A*, 2003, **107**, 7923.

[49] P. J. S. B. Caridade, S. B. Rodrigues, J. F. Sousa and A. J. C. Varandas, *J. Phys Chem. A*, 2005, **109**, 2356.

[50] P. J. S. B. Caridade, L. A. Poveda, S. B. Rodrigues and A. J. C. Varandas, *J. Phys Chem. A*, 2007, **111**, 1172.

[51] T. J. Francombe and G. Nyman, *J. Phys Chem. A*, 2007, **111**, 13163.

[52] T. V. Tscherbul, private communication.

[53] G. Knizia and H.-J. Werner, *JCP*, 2008, **128**, 154103.

[54] G. Knizia, T. B. Adler and H.-J. Werner, *JCP*, 2009, **130**, 054104.

[55] T. B. Adler, G. Knizia and H.-J. Werner, *JCP*, 2007, **127**, 221106.

[56] K. A. Peterson, T. B. Adler and H.-J. Werner, *J. Chem. Phys.*, 2008, **128**, 084102.

[57] T. Helgaker, W. Klopper, H. Koch and J. Noga, *J. Chem. Phys.*, 1997, **106**, 9639–9646.

[58] S. F. Boys and F. Bernardi, *Mol. Phys.*, 1970, **19**, 553.

[59] T. S. Ho and H. Rabitz, *J. Chem. Phys.*, 1996, **104**, 2584–2597.

[60] P. Soldán and J. M. Hutson, *J. Chem. Phys.*, 2000, **112**, 4415–4416.

[61] P. S. Żuchowski, R. Podeszwa, R. Moszynski, B. Jeziorski and K. Szalewicz, *J. Chem. Phys.*, 2008, **129**, 084101.

[62] D. J. Tozer and N. C. Handy, *J. Chem. Phys.*, 1998, **109**, 10180–10189.

[63] C. Adamo and V. Barone, *J. Chem. Phys.*, 1999, **110**, 6158–6170.

[64] L. M. C. Janssen, G. C. Groenenboom, A. van der Avoird, P. S. Zuchowski and R. Podeszwa, *J. Chem. Phys.*, 2009, **131**, 224314.

[65] C. R. Brazier, R. S. Ram and P. F. Bernath, *J. Mol. Spectrosc.*, 1986, **120**, 381–402.

[66] M. Mizushima, *Theory of Rotating Diatomic Molecules*, Wiley, New York, 1975.

[67] J. M. Hutson and S. Green, *MOLSCAT computer program, version 14*, distributed by Collaborative Computational Project No. 6 of the UK Engineering and Physical Sciences Research Council, 2006.

[68] R. V. Krems and A. Dalgarno, *J. Chem. Phys.*, 2004, **120**, 2296–2307.

[69] M. H. Alexander and D. E. Manolopoulos, *J. Chem. Phys.*, 1987, **86**, 2044.

[70] R. deCarvalho, J. Kim, J. D. Weinstein, J. M. Doyle, B. Friedrich, T. Guillet and D. Patterson, *Eur. Phys. J. D*, 1999, **7**, 289–309.

[71] R. V. Krems and A. Dalgarno, *Phys. Rev. A*, 2002, **66**, 012702.

[72] C. Ticknor and J. L. Bohn, *Phys. Rev. A*, 2005, **71**, 022709.

[73] Z. Pavlovic, R. V. Krems, R. Côté and H. R. Sadeghpour, *Phys. Rev. A*, 2005, **71**, 061402.

[74] M. S. Child, *Molecular Collision Theory*, Academic Press, London, 1974.

[75] G. F. Gribakin and V. V. Flambaum, *Phys. Rev. A*, 1993, **48**, 546.

[76] B. Gao, *Phys. Rev. A*, 1998, **58**, 1728–1734.

[77] B. Gao, *Phys. Rev. A*, 2000, **62**, 050702.

[78] F. H. Mies, *J. Chem. Phys.*, 1984, **80**, 2514–2525.

[79] F. H. Mies and P. S. Julienne, *J. Chem. Phys.*, 1984, **80**, 2526.